PHYSICAL REVIEW B **94**, 201119(R) (2016)

Tracking local magnetic dynamics via high-energy charge excitations in a relativistic Mott insulator

N. Nembrini,[1,2] S. Peli,[1,2] F. Banfi,[1] G. Ferrini,[1] Yogesh Singh,[3] P. Gegenwart,[4] R. Comin,[5,6] K. Foyevtsova,[5,6] A. Damascelli,[5,6] A. Avella,[7,8,9] and C. Giannetti[1]

[1]*I-LAMP & Department of Mathematics and Physics, Università Cattolica del Sacro Cuore, I-25121 Brescia, Italy*

[2]*Department of Physics, Università degli Studi di Milano, I-20133 Milano, Italy*

[3]*Indian Institute of Science Education and Research (IISER) Mohali, Knowledge City, Sector 81, Mohali 140306, India*

[4]*Experimental Physics VI, Center for Electronic Correlations and Magnetism, University of Augsburg, D-86159 Augsburg, Germany*

[5]*Department of Physics and Astronomy, University of British Columbia, Vancouver, British Columbia, Canada V6T 1Z1*

[6]*Quantum Matter Institute, University of British Columbia, Vancouver, British Columbia, Canada V6T 1Z4*

[7]*Dipartimento di Fisica "E. R. Caianiello", Università degli Studi di Salerno, I-84084 Fisciano (SA), Italy*

[8]*CNR-SPIN, UoS di Salerno, Via Giovanni Paolo II 132, I-84084 Fisciano (SA), Italy*

[9]*Unità CNISM di Salerno, Università degli Studi di Salerno, I-84084 Fisciano (SA), Italy*

(Received 2 June 2016; revised manuscript received 28 October 2016; published 22 November 2016)

We use time- and energy-resolved optical spectroscopy to investigate the coupling of electron-hole excitations to the magnetic environment in the relativistic Mott insulator Na_2IrO_3. We show that, on the picosecond time scale, the photoinjected electron-hole pairs delocalize on the hexagons of the Ir lattice via the formation of quasimolecular orbital excitations and the exchange of energy with the short-range-ordered zigzag magnetic background. The possibility of mapping the magnetic dynamics, which is characterized by typical frequencies in the THz range, onto high-energy (1–2 eV) charge excitations provides a platform to investigate, and possibly control, the dynamics of magnetic interactions in correlated materials with strong spin-orbit coupling, even in the presence of complex magnetic phases.

DOI: 10.1103/PhysRevB.94.201119

Addressing the way local charge excitations delocalize and interact with the magnetic environment is an urgent task in the study of correlated materials. The possible impacts range from the clarification of the microscopic origin of the spin correlations that give rise to exotic magnetic states in transition-metal oxides [1–5] to the possibility of photostimulating novel functionalities in materials in which the charge and magnetic excitations are strongly intertwined [6–8]. The family of 5*d* transition-metal oxides offers a particularly interesting playground to achieve these goals. In these materials, the on-site Coulomb repulsion U is reduced to $\approx$2 eV by the increased average radius of the orbitals and the spin-orbit coupling (SOC) interaction is pushed up to $\lambda_{SOC} \approx 0.7$ eV by the large mass of the metal atoms [9–11]. As a consequence of the interplay of U, λ_{SOC}, and the delocalization driven by the hopping, neither a local Mott-like picture nor a delocalized orbital scenario is fully appropriate to capture the rich phenomenology of these materials: from Mott insulating states in which the local moments have also orbital character [9,12] to exotic spin-liquid phases [1] driven by bond-directional magnetic interactions [4].

Here, we focus on the honeycomb relativistic Mott insulator Na_2IrO_3 and adopt a nonequilibrium approach [8]. We investigate how electron-hole excitations, photoinjected across the Mott gap [13,14], delocalize on the honeycomb lattice and release energy to the local magnetic background. Our experiment shows that the delocalization of local photostimulated charges is mediated by the excitations of specific quasimolecular orbitals (QMOs). The perfect symmetry matching between the relevant QMOs and the zigzag magnetic order allows the energy transfer to the magnetic background on the picosecond time scale. Exploiting the SOC-driven intertwining of magnetism and high-binding-energy electronic states, we show that the melting of the short-range zigzag order is mapped onto the modification of the optical properties in the near-infrared region. This finding provides a platform to track the magnetic dynamics in 5*d* transition-metal oxides, as well as in many other relativistic correlated materials.

In the honeycomb iridate Na_2IrO_3, the crystal-field-split Ir-t_{2g} orbitals host five electrons [15–17]. In the localized picture [9,18,19], SOC splits the t_{2g} manifold into completely filled $J_{\rm eff} = \frac{3}{2}$ levels and one half-filled $J_{\rm eff} = \frac{1}{2}$ state. The $J_{\rm eff} = \frac{1}{2}$ level is further split by the on-site Coulomb repulsion U into an empty upper Hubbard band (UHB) and an occupied lower Hubbard band (LHB), thus leading to a relativistic Mott insulator. This scenario provides a good explanation for both the measured insulating gap of $\approx$340 meV [12] and for the complex magnetic properties of the material, which exhibits strong magnetic correlations below $\Theta_{\rm corr} \approx 120$ K and a long-range-ordered zigzag phase below $T_N \approx 15$ K [17,20,21]. The large frustration parameter $\Theta_{\rm corr}/T_N \approx 8$ [17] and the evidence of bond-directional magnetic interactions described by the Kitaev model [4] suggest the tendency to form a low-temperature spin-liquid phase out of which the zigzag order emerges.

On the other hand, the large oxygen-mediated hopping term ($\approx$250 meV) between neighboring Ir atoms drives a very effective electronic delocalization over the Ir hexagons. As a consequence, quasimolecular orbitals (QMOs), built from linear combinations of Ir-t_{2g} Wannier functions, emerge as the natural basis for describing the electronic properties of Na_2IrO_3 [22,23]. It has been recently demonstrated that the concept of QMOs is the key to rationalize the outcome of *ab initio* band-structure calculations [22,23] and accounts for the manifold of structures observed in the 0.3–2 eV energy range via photoemission and optical spectroscopy [12,24].

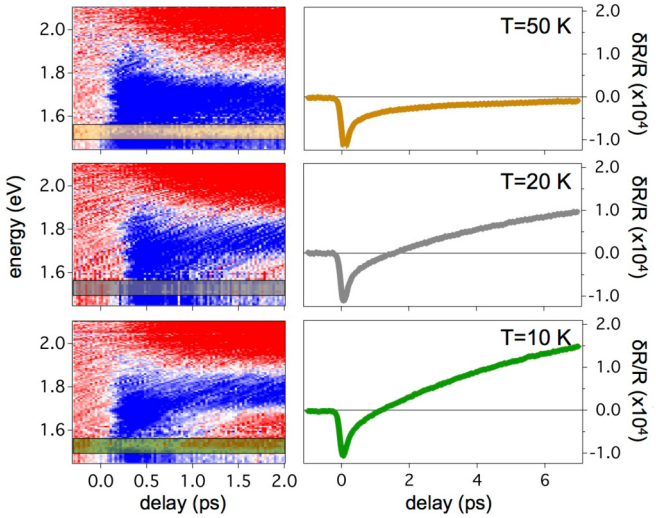

FIG. 1. Left: Energy- and time-resolved reflectivity measurements on Na_2IrO at different temperatures. The color scale indicates positive (negative) $\delta R(\omega,t)/R$ in red (blue). The pump fluence was varied between 10 and 40 μJ/cm^2. Right: Time traces, i.e., constant-energy cuts, extracted from $\delta R(\omega,t)/R$ for $t = 2$ ps at $T = 50$, 20, and 10 K.

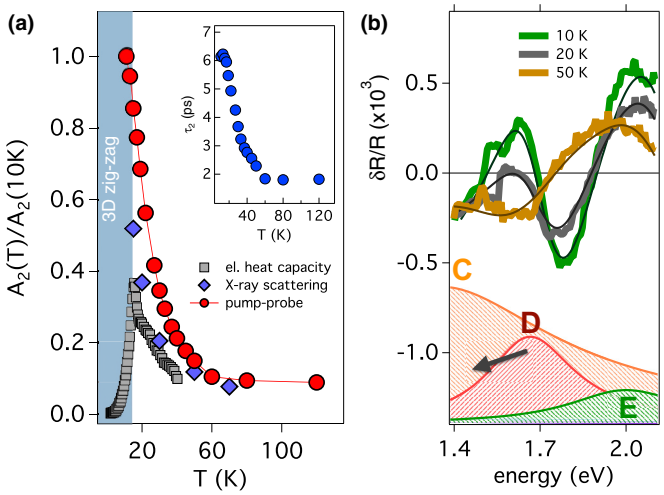

FIG. 2. (a) Temperature dependence of the amplitude (red dots) of the slow exponential function A_2 renormalized to the value at $T = 10$ K. The values were extracted by the exponential fitting of the $\delta R(\omega,t)/R$ time traces for $\hbar\omega = 1.5$ eV and by single-color time-resolved reflectivity measurements with a fluence of 0.5–10 μJ/cm^2. The pump-probe data are compared to the magnetic heat capacity (gray squares, taken from Ref. [17]), i.e., $\Delta C = C(T) - C_{\rm lat}(T)$, where $C(T)$ is the total heat capacity and and $C_{\rm lat}(T)$ the lattice heat capacity; and to the total integral of the H scan of the magnetic peak at $\mathbf{Q} = (0\ 1)$, as measured by resonant inelastic x-ray scattering in Ref. [4] (blue diamonds, taken from Fig. S3 in the Supplemental Material). Both the heat capacity and the intensity of the scattering signal at the magnetic peak are reported in arbitrary units, to allow direct comparison with time-resolved data on the same graph. The blue area indicates the region of long-range three-dimensional zigzag order below $T_{\rm N}$. The inset reports the temperature dependence of the time constant τ_2 of the slow exponential function. (b) Energy traces extracted from $\delta R(\omega,t)/R$ for $t = 2$ ps. The black lines represent the fit to the data of a differential dielectric function in which only the oscillator corresponding to the optical transition D has been modified. The fitting procedure returns a redshift of $\approx$10 meV for the oscillator D, at a pump fluence of $\approx$10 μJ/cm^2.

Broadband pump-probe optical spectroscopy is performed on high-quality Na_2IrO_3 crystals [17]. While the pump pulse ($\hbar\omega_p = 1.55$ eV photon energy) is used to photoinject local electron-hole excitations across the Mott gap, the broadband probe snaps the dynamics of the optical transitions in the range 1–2 eV, that corresponds to large binding-energy QMOs. The time- and energy-resolved reflectivity variation $[\delta R(\omega,t)/R]$ measurements have been performed by exploiting the supercontinuum white light produced by a photonic crystal fiber seeded by a cavity-dumped (543 kHz repetition rate) Ti:sapphire oscillator (for details, see Refs. [25,26]). This configuration allowed us to perform measurements in the low-excitation regime and avoid the local heating of the sample [27]. In Fig. 1 (left panels), we report the two-dimensional $\delta R(\omega,t)/R$ plots taken at three different temperatures. Following the pump excitation at $t = 0$, the $\delta R(\omega,t)/R$ signal is characterized by a temperature-independent response, which turns from positive (red) to negative (blue) at $\hbar\omega \approx 1.8$ eV. This response can be attributed to a thermomodulation effect [28] that results in the broadening of the interband transitions involving energy scales >2 eV. More interestingly, a different positive component appears a few picoseconds after the excitation in a narrow spectral region (1.4–1.7 eV) when $T_{\rm N}$ is approached. The dynamics of this additional component is clearly evidenced by the right panels of Fig. 1, which report the time traces extracted from the $\delta R(\omega,t)/R$ signal at $\hbar\omega \approx 1.55$ eV. On the picosecond time scale, the dynamics of the $\delta R(t)/R$ signal is characterized by a very slow buildup time of a positive component, whose amplitude increases at low T. In order to systematically extract the amplitude and timescale of this component, we performed a simple double-exponential fit of the function $A_1 \exp(-\frac{t}{\tau_1}) + A_2 \exp(-\frac{t}{\tau_2})$ to the data. While both A_1 and τ_1 are found to be temperature independent [27] in the entire explored temperature range (10–120 K), the amplitude and time scale of the second component dramatically increase at low temperatures, as shown in Fig. 2(a) (red dots). To rule out possible artifacts related to impulsive heating, that could be particularly relevant at low temperatures, very-low-fluence (0.1–10 μJ/cm^2) single-color ($\hbar\omega_p = 1.55$ eV) time-resolved reflectivity measurements were performed [27]. The values of A_2 and τ_2 are found to be constant up to fluences of 10 μJ/cm^2, thus demonstrating that the slowing down of the second dynamics is a genuine physical effect related to the progressive onset of magnetic correlations on approaching $T_{\rm N}$.

These results are in agreement with single-color measurements reported in Refs. [13,14], which suggested the following two-step picture: (i) On the $\tau_1 \approx 200$ fs time scale, the high-energy electron-hole excitations created by the 1.55 eV pump pulse relax through electron-electron interactions and the coupling with optical phonons, thus leading to the fast accumulation of doublons (i.e., doubly occupied Ir sites) and holons (i.e., unoccupied Ir sites) at the bottom (top) of the UHB (LHB); (ii) the interaction with the locally ordered magnetic environment, characterized by the combination of Kitaev and

Heisenberg-type correlations, drives the binding of the holons and doublons into local excitons, whose binding energy grows with their distance [13]. As a consequence of the strong dynamical constraints, the delocalization of the holon-doublon pairs is expected to be strongly delayed and to be eventually effective only on the picosecond time scale [13].

While the dynamics of the local excitons can be rationalized within the $J_{\rm eff}$ model [13], its relationship with the modification of the high-energy optical properties remained obscure so far. The frequency resolution of the data reported in this work allows us to make a fundamental step beyond single-color measurements and to address both the origin of the observed signal at $\approx$1.6 eV and the way the local excitons delocalize on the Ir hexagons and release their excess energy to the zigzag magnetic background. In particular, the results presented in Figs. 1 and 2(a) are characterized by two important features. First, the $\delta R(\omega,t)/R$ signal in the 1.4–1.7 eV spectral range is detected at temperatures well above $T_{\rm N}$ [see Fig. 2(a)], while no divergence of A_2 and τ_2 is observed at T_N. This finding suggests that the relaxation dynamics of the excitons is slowed down by *short-range* zigzag correlations [14]. This observation can be corroborated by comparing the temperature dependence of the A_2 component to the outcomes of equilibrium techniques. In Fig. 2(a), we report the electronic contribution to the heat capacity measured in Ref. [17]. The broad tail extending up to 60 K was interpreted [17] as the signature of the presence of short-range magnetic correlations well above $T_{\rm N}$. More recently, the existence of zigzag correlations at temperatures above the long-range magnetic phase transition has been directly supported by resonant inelastic x-ray scattering measurements [4]. The temperature dependence of the magnetic diffraction peak, reported in Fig. 2(a), directly demonstrates the persistence of zigzag magnetic correlations, with a correlation length (ξ) of 1.6–1.8 nm, at least up to $\approx$70 K. Importantly, the temperature dependence of the A_2 component in the $\delta R(t)/R$ signal almost perfectly overlaps with that of the short-range zigzag correlations [see Fig. 2(a)]. This observation strongly supports the interpretation of the slow dynamics observed in the pump-probe experiment as the time needed by the nonequilibrium distribution of electron-hole excitations to couple to the zigzag order on a spatial scale ξ, eventually leading to its (partial) melting. Second, the appearance of the slow $\delta R(t)/R$ signal is confined to a narrow frequency range. This suggests that the delocalization of the doublons and the consequent melting of the zigzag order selectively affect a specific high-energy QMO. Quantitatively, this can be demonstrated by a differential fitting procedure that builds on a multi-Lorentzian model of the equilibrium dielectric function [27]. Both the position and the amplitude of the five oscillators used to reproduce the dielectric function perfectly map the transitions expected in the QMOs picture [24] (for a detailed discussion, see Ref. [27]). Importantly, the spectrally narrow positive component that appears at low temperatures is solely related to a modification of a specific oscillator (labeled D as shown in Fig. 2), which thus unveils a direct interplay between the melting of the zigzag order and one of the QMOs at binding energy $\geqslant$1 eV.

To shed light onto the relation between magnetism and QMOs, the electronic band structure of Na_2IrO_3 has been calculated by *ab initio* relativistic density functional theory (DFT), performed through the linearized augmented plane wave (LAPW) method as implemented in the full-potential code WIEN2K. As extensively discussed in several works [22–24,29], the DFT-calculated density of states (DOS) presents five separated bands which are strongly reminiscent of the QMOs. The six QMOs localized on a particular hexagon can be grouped into the lowest-energy B_{1u} singlet, the two doublets E_{1g} and E_{2u}, and the highest-energy A_{1g} singlet [22]. SOC mixes the three QMOs closer to the Fermi energy, splits the doublets, and leads to a suppression of the density of states at the Fermi level [12,22,23]. This suppression further evolves into the experimental gap when the Coulomb repulsion $U_{\rm eff}$ is considered [12,24].

Interestingly, the QMO representation has a strong connection with the zigzag magnetic order emerging at low temperature. Figure 3 shows that suitable linear QMO combinations preserve both the spatial arrangement and the magnetic polarization of the zigzag ordering. In particular, the $E^{(1)}_{1g} \pm E^{(2)}_{2u}$ combinations (dark red curves in Fig. 3), which are mainly located at $\approx$1 eV binding energy and account for the optical transition D, are almost fully polarized according to the zigzag pattern. Furthermore, they are characterized by a nonzero overlap with both the occupied states right below the Fermi level and the empty states at $\approx$+0.3 eV (see Fig. S1 of the Supplemental Material), thus constituting the perfect link between the low-energy dynamics and the high-energy electronic properties.

The combination of nonequilibrium optics and *ab initio* calculations provides a comprehensive picture of the delocalization of the holon-doublon pairs and of the energy exchange with a magnetic background (see Fig. 4). The holon-doublon pairs are initially confined by the dynamical constraints given by the topology of the zigzag magnetic correlations [13]. On the picosecond time scale, the local pairs degrade via the delocalization on the Ir hexagons and form QMO-like charge excitations that are delocalized over a length scale of the order of 1.6–1.8 nm. In particular, the strong $E^{(1)}_{1g} \pm E^{(2)}_{2u}$ character of the empty states at the bottom of the UHB (see Fig. 3) allows us to identify this specific QMO combination as the channel for the energy transfer between charge excitations and the magnetic background. Considering the almost full zigzag polarization of the $E^{(1)}_{1g} \pm E^{(2)}_{2u}$ QMOs (see Fig. 3), we argue that the excess charge excitations in the UHB are intrinsically associated with the weakening of the zigzag order, thus driving an effective heating of the spin background. As a feedback, the perturbation of the zigzag magnetic order is expected to particularly affect the QMOs combinations that exhibit the same spatial pattern and spin polarization. Specifically, the partial quench of the zigzag magnetic correlations leads to the modification of the strongly coupled $E^{(1)}_{1g} \pm E^{(2)}_{2u}$ QMOs at ≈ -1 eV binding energy, thus allowing one to map the low-energy magnetic dynamics onto the variation of the optical properties at 1.4–1.7 eV.

Our results have also a wider impact on the physics of relativistic correlated materials. In the case of honeycomb iridates, our results demonstrate that the efficacy of the fully localized ($J_{\rm eff}$) and quasidelocalized (QMO) scenarios strongly depends on the energy scale considered: While the

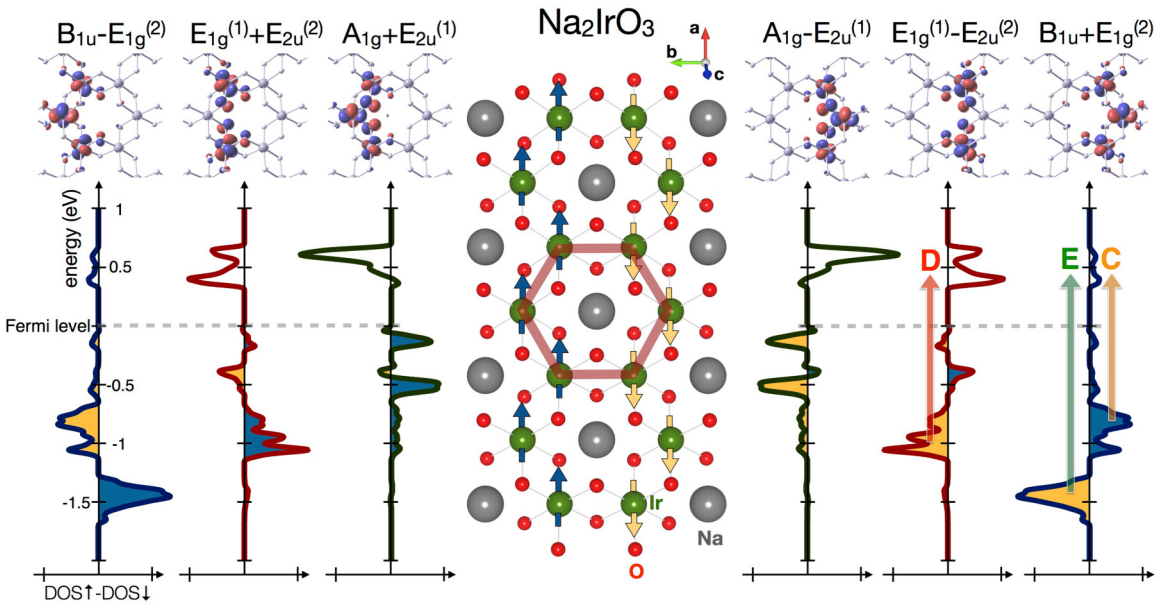

FIG. 3. QMO description of the Na_2IrO_3 band structure. The *ab initio* total spin-resolved DOS is projected onto suitable combinations of the QMOs. The six linear combinations showed in the figure reproduce both the spatial (see the wave functions reported in the top panel) and the magnetic polarization (see the net polarizations, defined as the differences between the QMO-projected spin-up and spin-down DOS, reported in the bottom panel) of the zigzag ordered ground state. The on-site Coulomb repulsion is accounted for by a $U_{\text{eff}} = 2.4$ eV correction that generates the experimental insulating gap [12,24]. The Na_2IrO_3 honeycomb lattice structure is reported in the central panel. The magnetic zigzag ordered phase is indicated by the blue (spin-up) and yellow (spin-down) arrows. The correspondence between the optical transitions C, D, E reported in Fig. 2 and the QMOs is highlighted by the colored arrows.

low-energy magnetic dynamics is compatible with a picture of localized moments characterized by bond-dependent (Kitaev) interactions, QMOs are the effective building blocks of the physics at binding energies larger than ≈1 eV. More in general, the interplay of the on-site U and SOC intrinsically leads to the intertwining between the magnetic order and the high-energy electronic states in multiorbital systems, independently of the formation of QMOs. Therefore, the possibility of mapping the demagnetization processes onto specific optical transitions in the near-infrared/visible energy range could be extended to a variety of correlated materials and frustrated magnets, such as pyrochlore iridates and other systems that exhibit exotic spin-liquid phases driven by Kitaev interactions. Conversely, the resonant excitation of QMOs or other large binding-energy electronic states in relativistic correlated materials on a time scale faster than the coupling to the magnetic degrees of freedom can be used to trigger emergent excitations that can interact with a *cold* magnetic background and can be directly accessed by ultrafast techniques.

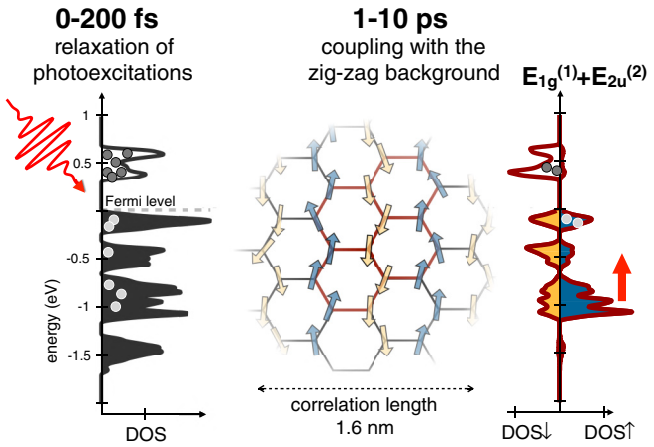

FIG. 4. Cartoon of the relaxation processes after the initial photoexcitation. The left panel reports the *ab initio* total DOS of the occupied and unoccupied states. The right panel shows the spin-resolved DOS of the $E_{1g}^{(1)} + E_{2u}^{(2)}$ QMO combination. We note that a coherence length as short as 1.6–1.8 nm coincides with the length scale necessary for a full tight-binding description of the Na_2IrO_3 band structure in terms of QMOs [22].

We thank M. Capone, I. Elfimov, G. Jackeli, G. Khaliullin, and I. Mazin for fruitful discussions. C.G., F.B., and G.F. acknowledge support from Università Cattolica del Sacro Cuore through D1, D.2.2, and D.3.1 grants. F.B. acknowledges financial support from Ministero dell'Istruzione, dell'Università e della Ricerca (MIUR) through the ULTRANANO project (Project No. RBFR13NEA4) within the Futuro in Ricerca 2013 Grant and from Fondazione E.U.L.O. The work at Augsburg University is supported by the Deutsche Forschungsgemeinschaft (DFG) through Projects No. TRR-80 and No. SPP 1666. The work at UBC was supported by the Killam, A. P. Sloan, A. von Humboldt, and NSERC's Steacie Memorial Fellowships (A.D.), the Canada Research Chairs Program (A.D.), NSERC, CFI, and CIFAR Quantum Materials. Y.S. acknowledges the Department of Science and Technology (DST) of the Ministry of Science and Technology (India) for support through Ramanujan Grant No. SR/S2/RJN-76/2010 and through DST Grant No. SB/S2/CMP-001/2013.

[1] L. Balents, Nature (London) **464**, 199 (2010).
[2] D. Pesin and L. Balents, Nat. Phys. **6**, 376 (2010).
[3] Y. Tokiwa, J. J. Ishikawa, S. Nakatsuji, and P. Gegenwart, Nat. Mater. **13**, 356 (2014).
[4] S. Hwan Chun, J.-W. Kim, J. Kim, H. Zheng, C. C. Stoumpos, C. D. Malliakas, J. F. Mitchell, K. Mehlawat, Y. Singh, Y. Choi, T. Gog, A. Al-Zein, M. M. Sala, M. Krisch, J. Chaloupka, G. Jackeli, G. Khaliullin, and B. J. Kim, Nat. Phys. **11**, 462 (2015).
[5] M. P. M. Dean, Y. Cao, X. Liu, S. Wall, D. Zhu, R. Mankowsky, V. Thampy, X. M. Chen, J. G. Vale, D. Casa, J. Kim, A. H. Said, P. Juhas, R. Alonso-Mori, J. M. Glownia, A. Robert, J. Robinson, M. Sikorski, S. Song, M. Kozina, H. Lemke, L. Patthey, S. Owada, T. Katayama, M. Yabashi, Y. Tanaka, T. Togashi, J. Liu, C. Rayan Serrao, B. J. Kim, L. Huber, C.-L. Chang, D. F. McMorrow, M. Forst, and J. P. Hill, Nat. Mater. **15**, 601 (2016).
[6] A. Kirilyuk, A. Kimel, and T. Rasing, Rev. Mod. Phys. **82**, 2731 (2010).
[7] T. Kubacka *et al.*, Science **343**, 1333 (2014).
[8] C. Giannetti, M. Capone, D. Fausti, M. Fabrizio, F. Parmigiani, and M. Mihailovic, Adv. Phys. **65**, 58 (2016).
[9] B. J. Kim, H. Jin, S. J. Moon, J.-Y. Kim, B.-G. Park, C. S. Leem, J. Yu, T. W. Noh, C. Kim, S.-J. Oh, J.-H. Park, V. Durairaj, G. Cao, and E. Rotenberg, Phys. Rev. Lett. **101**, 076402 (2008).
[10] G. Jackeli and G. Khaliullin, Phys. Rev. Lett. **102**, 017205 (2009).
[11] A. Shitade, H. Katsura, J. Kuneš, X.-L. Qi, S.-C. Zhang, and N. Nagaosa, Phys. Rev. Lett. **102**, 256403 (2009).
[12] R. Comin, G. Levy, B. Ludbrook, Z.-H. Zhu, C. N. Veenstra, J. A. Rosen, Y. Singh, P. Gegenwart, D. Stricker, J. N. Hancock, D. van der Marel, I. S. Elfimov, and A. Damascelli, Phys. Rev. Lett. **109**, 266406 (2012).
[13] Z. Alpichshev, F. Mahmood, G. Cao, and N. Gedik, Phys. Rev. Lett. **114**, 017203 (2015).
[14] J. P. Hinton, S. Patankar, E. Thewalt, A. Ruiz, G. Lopez, N. Breznay, A. Vishwanath, J. Analytis, J. Orenstein, J. D. Koralek, and I. Kimchi, Phys. Rev. B **92**, 115154 (2015).
[15] I. Felner and I. Bradaric, Physica B **311**, 195 (2002).
[16] H. Kobayashi, M. Tabuchi, M. Shikano, H. Kageyama, and R. Kanno, J. Mater. Chem. **13**, 957 (2003).
[17] Y. Singh and P. Gegenwart, Phys. Rev. B **82**, 064412 (2010).
[18] J. Chaloupka, G. Jackeli, and G. Khaliullin, Phys. Rev. Lett. **105**, 027204 (2010).
[19] J. Chaloupka, G. Jackeli, and G. Khaliullin, Phys. Rev. Lett. **110**, 097204 (2013).
[20] F. Ye, S. Chi, H. Cao, B. C. Chakoumakos, J. A. Fernandez-Baca, R. Custelcean, T. F. Qi, O. B. Korneta, and G. Cao, Phys. Rev. B **85**, 180403 (2012).
[21] S. K. Choi, R. Coldea, A. N. Kolmogorov, T. Lancaster, I. I. Mazin, S. J. Blundell, P. G. Radaelli, Y. Singh, P. Gegenwart, K. R. Choi, S.-W. Cheong, P. J. Baker, C. Stock, and J. Taylor, Phys. Rev. Lett. **108**, 127204 (2012).
[22] I. I. Mazin, H. O. Jeschke, K. Foyevtsova, R. Valentí, and D. I. Khomskii, Phys. Rev. Lett. **109**, 197201 (2012).
[23] K. Foyevtsova, H. O. Jeschke, I. I. Mazin, D. I. Khomskii, and R. Valentí, Phys. Rev. B **88**, 035107 (2013).
[24] Y. Li, K. Foyevtsova, H. O. Jeschke, and R. Valentí, Phys. Rev. B **91**, 161101 (2015).
[25] C. Giannetti, F. Cilento, S. D. Conte, G. Coslovich, G. Ferrini, H. Molegraaf, M. Raichle, R. Liang, H. Eisaki, M. Greven, A. Damascelli, D. van der Marel, and F. Parmigiani, Nat. Commun. **2**, 353 (2011).
[26] F. Cilento, C. Giannetti, G. Ferrini, S. Dal Conte, T. Sala, G. Coslovich, M. Rini, A. Cavalleri, and F. Parmigiani, Appl. Phys. Lett. **96**, 021102 (2010).
[27] See Supplemental Material at http://link.aps.org/supplemental/10.1103/PhysRevB.94.201119 for technical details on the DFT calculations, including the relation between the optical conductivity and the calculated band structure, as well as additional details on the differential fitting and on the experiment, including the effect of local heating and the sub-ps dynamics.
[28] C.-K. Sun, F. Vallée, L. H. Acioli, E. P. Ippen, and J. G. Fujimoto, Phys. Rev. B **50**, 15337 (1994).
[29] I. I. Mazin, S. Manni, K. Foyevtsova, H. O. Jeschke, P. Gegenwart, and R. Valentí, Phys. Rev. B **88**, 035115 (2013).